GEOPHYSICAL RESEARCH LETTERS, VOL. 28, NO. 2, PAGES 219-222, JANUARY 15, 2001

Particle-in-cell simulations of the lunar wake with high phase space resolution

Paul C. Birch and Sandra C. Chapman

Space and Astrophysics Group, Physics Department, University of Warwick, UK

Abstract. The evolution of the lunar wake in simplified geometry can be simulated via a $1\frac{1}{2}$D electromagnetic particle-in-cell code. By using a sufficient number of particles per cell, we are able, for the first time, to resolve the full phase space dynamics of both electrons and ions. This simulation begins immediately downstream of the moon, before the solar wind has infilled the wake region, then evolves in the solar wind rest frame. The electrons immediately begin to move into the void but are trapped by two potential wells, thus generating vortices in phase space on both sides of the wake, between which counter-streaming electron beams interact. Ion beams are generated after the lighter electrons have moved into the void, creating a two-stream distribution which mixes in phase space due to the potentials created by the electron two-stream instability. Other structures are also evident. The simulations are consistent with both WIND observations and the results of earlier electrostatic simulations which focus only on the ion dynamics.

1. Introduction

The solar wind flows past the moon, resulting in a wake structure behind it. Since the moon has no magnetic field or ionosphere, the particles that collide with the moon will be absorbed and removed from the distribution. Directly behind the moon there will be a void in which no solar wind particles are present. Following the WIND spacecraft's encounter with the lunar plasma wake on December 27, 1994, a number of descriptions of the structure and dynamics of the wake have been produced. Observations by WIND showed many characteristics of the wake at about 6.5 lunar radii (R_L) downstream. These include significant ion and electron depletions, increased electron temperature, counter-streaming ion beams and rarefaction waves travelling away from the wake. Also detected were a number of electromagnetic and electrostatic waves [*Ogilvie et al.*, 1996; *Bosqued et al*, 1996; *Owen et al.*, 1996; *Kellogg et al.*, 1996; *Farrell et al.*, 1996; *Farrell et al.*, 1997; *Bale et al.*, 1997; *Bale*, 1997].

Paper number 2000GL011958.
0094-8276/01/2000GL011958$05.00

The process by which the wake infills was considered analytically by *Ogilvie et al.*, [1996]. The observed counter-streaming ion beams set up a two-stream distribution in the centre of the wake, thus creating an instability. Once the instability has reached its saturated state, the beams will begin folding in phase space and eventually produce a monotone-decreasing distribution. A simple simulation of a plasma void [*Farrell et al.*, 1998] produced a description of the lunar wake, consistent in some respects with the observations made with WIND at 6.5 R_L. Due to the number of particles per cell used by *Farrell et al.*, [1998], only the ion dynamics were studied in detail. Ion beams were formed and subsequently disrupted by the two-stream instability. A density rarefaction wave was also produced, as predicted and observed by *Ogilvie et al.*, [1996].

We present results from a similarly geometrically simple $1\frac{1}{2}$D kinetic simulation of the lunar wake, but with significantly more particles per cell, thereby fully resolving both ion and electron phase space structure and dynamics for the first time. This enables a more complete comparison with the WIND observations, in particular including the full electron dynamics. Resolving the electron dynamics also allows a more complete understanding of the ion dynamics.

2. The Particle-in-Cell Simulation

The simulation was produced using a thoroughly tested, self consistent, fully relativistic, collisionless $1\frac{1}{2}$D particle-in-cell (PIC) code. In such simulations, the ion and electron distribution functions are represented by a collection of "superparticles". These "superparticles", along with the electric and magnetic fields, can exhibit both full ion and electron kinetics. The velocities of the "superparticles" and the fields have vector components in three dimensions, but are a function of one configuration space dimension, and time. Known as $1\frac{1}{2}$D simulations, since $\nabla \cdot \underline{B} = 0$, the component of $\underline{B}$ along the simulation is constant. The number of superparticles directly determines the phase space resolution of the simulation, here we use $\sim$ 2500 per cell compared with $\sim$ 40 per cell in *Farrell et al.*, [1998].

Figure 1 shows the geometry of the simulation which is similar to that used by *Farrell et al.*, [1998]. The simulation box begins directly behind the moon, perpendicular to the solar wind flow (-X direction) and parallel to the IMF (Y direction). A higher dimensional

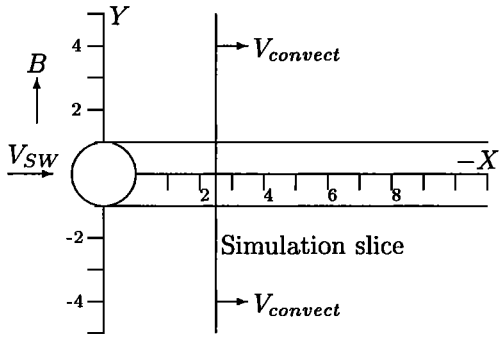

Figure 1. Simulation geometry.

simulation would be required to describe the lunar wake when the IMF is at oblique angles, and bulk flows other than in the solar wind flow direction as the simulation is performed in the rest frame of the solar wind with zero convection electric field. The IMF will pass almost unaltered through the moon since the moon can be assumed to be a perfect insulator and therefore no currents can flow to change the field. The simulation then begins with a void in an otherwise Maxwellian distribution of ions and electrons which mimics the removal of solar wind particles by the moon. Full shadowing is appropriate since the electron and ion gyroradii (95m and 417m) are significantly smaller than one lunar radius (~1738km). Possible crustal remnant fields which are of the order of the IMF at the lunar surface are neglected in this simple 1D simulation. As we move with the solar wind, simulation run time can be equated to a distance behind the moon, effectively building up a 2D picture of the wake, provided the IMF and solar wind flow remain constant.

We choose an ion to electron mass ratio of 20 in order to evolve both ion and electron dynamics. This alters the simulation's ion plasma frequency and ion thermal velocity. Since the actual solar wind velocity is 25 times the ion thermal velocity v_{thi}, the simulation also requires this relationship. Thus, the distance behind the moon is given by, $X = V_{conv}t$, where $V_{conv} = 25v_{thi}$ and t is measured in plasma periods, ω_{pe}^{-1}. This is equivalent to $X = 0.0437R_L t$ where t is in plasma periods and R_L is the radius of the moon, i.e. half the width of the void. In reality, $v_{the} > V_{conv} > v_{thi}$; this may affect the magnitude of the potential and effectively rescales $X = V_{conv}t$.

With periodic boundary conditions, the simulation run time is limited to the time for the most energetic electrons to reach the boundaries and is $10^3\ \omega_{pe}^{-1}$ with a 2048 grid cell simulation box (grid cell = Debye length, λ_D) and a void of $256\lambda_D$ in the centre (corresponding to a box length of 214.5 electron gyroradii, 8.4 $\frac{c}{\omega_{pe}}$). Larger voids (up to $512\lambda_D$) have also been considered.

3. Results of the Simulations

Figure 2 shows how the electron density evolves. The age of the simulation slice is equated to a distance behind the moon, along the X axis. The initial void has begun to infill by 7 R_L. A rarefaction wave travelling away from the wake is evident from $t = 0$ moving at the ion sound speed, as predicted by *Ogilvie et al.*, [1996]. Two high density regions can be seen to form on both edges of the wake. By examining the electric potentials calculated from the electric field data, it is apparent that two potential wells form on either side of the wake, trapping the majority of the electrons (see Figure 3). The potential wells are dynamic and quasi-periodically allow electrons to escape, resulting in the increased electron densities moving away from the wake or towards the centre that can be seen in figure 2. These clumps of electrons travel faster than the electron thermal velocity since it will be the most energetic electrons which escape when an edge of the potential well is lowered. These perturbations in electron density also appear in the electric field (not shown here). The phase space of the electrons shows how the potential wells capture the electrons and confine them to the two regions in the wake (Figure 4). Initially, the electrons move towards the centre of the wake, setting up the two potential wells. Note that these potential wells are self-consistent: trapping the electrons which set them up. These wells trap all but the most energetic electrons; the latter form two streams at the wake centre. This two-stream distribution is unstable and subsequently begins to mix in phase space, generating phase space vortices and creating more potentials which trap the electrons. These vortices grows as more electrons are captured, eventually coalescing with each other. The asymmetry is due to the nonlinearity of the fully evolved electron two-stream instability, resulting in one of the vortices dominating the others.

The characteristic ion time scales are significantly longer than the electron time scales, due to their higher mass, so the ion dynamics evolve in the presence of the electric potentials created by the electrons. The potentials exclude all but the high energy tail of the ion distribution from the wake; these form ion beams (Figure 4). After 160 ω_{pe}^{-1} or 7 R_L, the ion beams meet in the centre of the wake and flow past one another. This creates a counter-streaming ion beam distribution as detected by WIND [*Ogilvie et al.*, 1996]. The beams are subsequently distorted, however here this is not due to the ion two-stream instability, but is controlled by the electric potentials created by the electron two-stream instability. The timescale for phase mixing due to ion two-stream instability would be $\sim 6 \times 10^3 \omega_{pe}^{-1}$ in our simulation. This process does not have sufficient time to thermalize the ions in our simulation. Fluctuations in ion density with corresponding fluctuations in electric field (not shown here) are also found travelling away from the wake structure close to the ion sound speed and the ion thermal velocity. These coincide with times when the ion beams exit the wake.

Further simulations have been carried out using a larger initial void. Rather than a $256\lambda_D$ void as shown here, a $512\lambda_D$ void was used. With this alteration, the

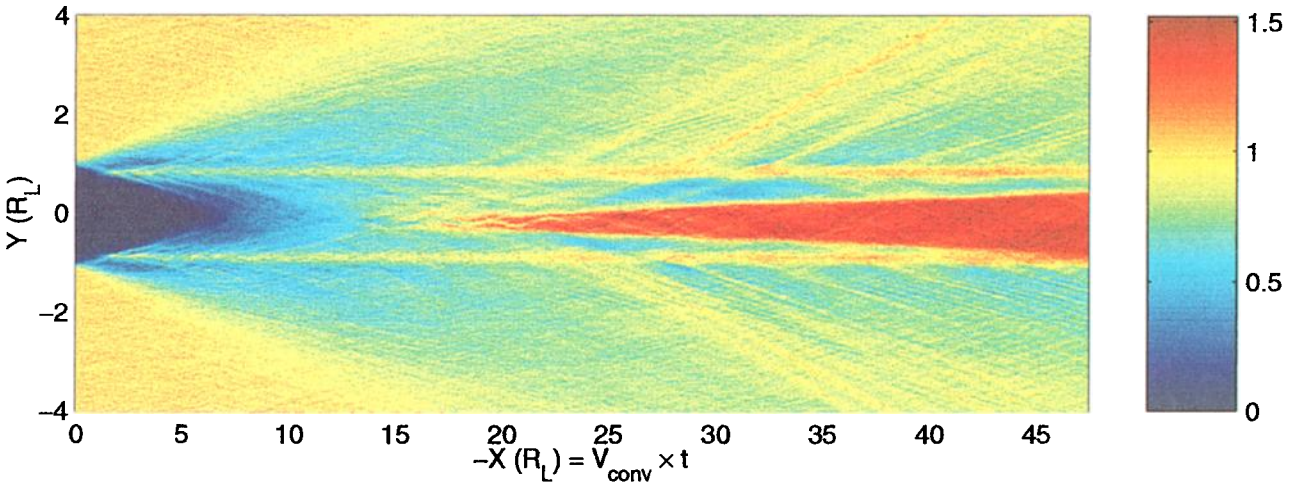

Figure 2. Electron density evolution shows distance along simulation box $Y(R_L)$ against time (distance behind moon) $X(R_L)$ with density normalised to the ambient solar wind density. The simulation box extends to $\pm 8R_L$.

electrons still move into the wake, then set up two potentials at the edges, the same size as previously. Then the same counter-streaming electron beams are set up, however there is more space between the edge potentials, allowing more phase space vortices to be generated by the electron two-stream instability. These vortices grow and coalesce to fill the wake. The ion beam evolution again is controlled by the potential generated by the electrons. Given that the moon is about $3.5 \times 10^5 \lambda_D$ in diameter, one would expect many phase space vortices to be generated between the two edge potentials, which grow and coalesce to fill the wake.

4. Comparison of Results with WIND Observations

The WIND spacecraft passed through the wake about 6.5 R_L behind the moon, which can be equated to about 150 ω_{pe}^{-1} in the simulation. Figure 5 shows the simulation after 150 ω_{pe}^{-1} which can be compared with the data from WIND; in particular, figure 1 in *Ogilvie et al.*, [1996], which shows plasma and magnetic field parameters observed during the lunar wake crossing.

The simulated ion density is in good agreement with the WIND data given the caveat that the solar wind ion density dropped while WIND was in the wake, whereas the simulation assumes that the solar wind has constant ion and electron densities. WIND also detected

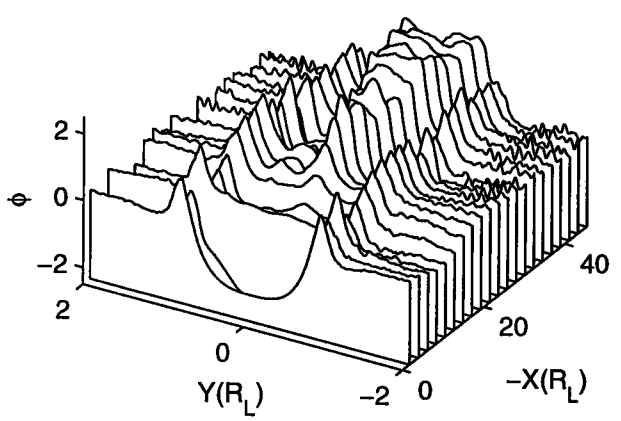

Figure 3. A stack plot of electric potentials (in units of eV) calculated from electric field data, plotted against distance along simulation box $Y(R_L)$ and time transformed to a distance behind the moon $X(R_L)$, beginning at $40\omega_{pe}^{-1} = 1.75R_L$, then every $50\omega_{pe}^{-1} = 2.19R_L$. The simulated obstacle is ~1400 times smaller than the moon, so that the total potential drop is substantially less in the simulation.

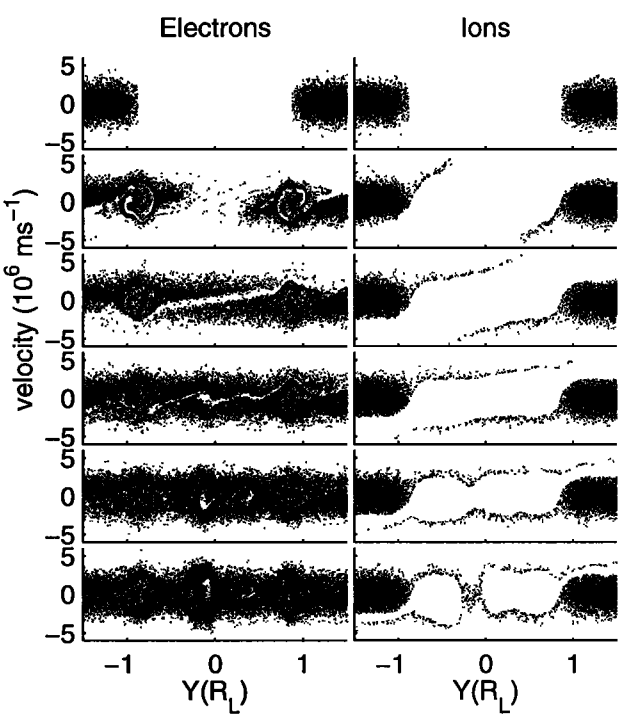

Figure 4. Cut in electron and ion phase space; plotted are positions along simulation box $Y(R_L)$ against velocities along simulation box (v_Y, in units of $10^6 ms^{-1}$), beginning with the top plot at $0\omega_{pe}^{-1} = 0R_L$, then every $100\omega_{pe}^{-1} = 4.38R_L$. Ion velocities multiplied by $\sqrt{20}$.

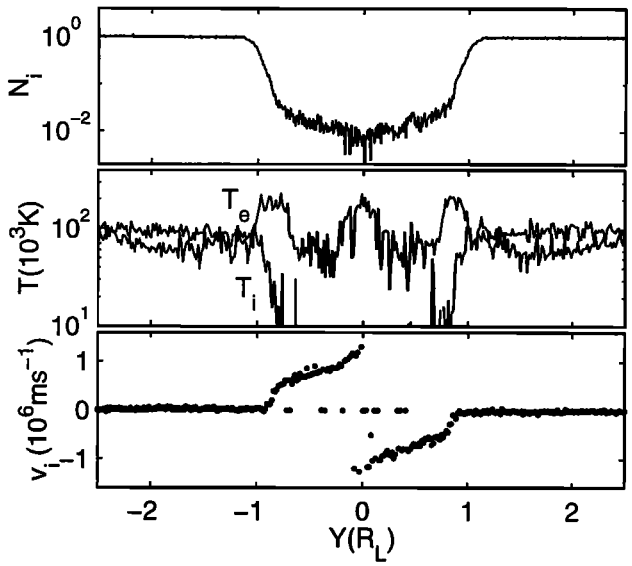

Figure 5. Simulation results at 6.5 R_L showing: Ion density (normalised to the ambient solar wind ion density), ion / electron temperatures (units of 10^3K) and ion speed (units of $10^6 ms^{-1}$), plotted against distance along simulation box Y(R_L). For comparison with WIND data, in particular fig. 1 in *Ogilvie et al.*, [1996].

the rarefaction waves, in agreement with the analytical approach by *Ogilvie et al.*, [1996] and with simulations. The observed and simulated temperatures are in reasonable agreement. The electron temperature rises in the wake according to both WIND and the simulations. WIND found the electron temperature peaks near the centre whereas the simulations can resolve peaks where the phase space vortices are created. The observed ion temperatures are difficult to compare since the ion distribution at this time is essentially two beams. The ion distribution sampled by WIND clearly shows counter-streaming beams, which we also find in the simulation.

5. Conclusion

By using a high resolution simulation, we are able, for the first time, to fully resolve the electron phase space dynamics and thus obtain a more complete understanding of the ion dynamics in the lunar wake. This yields more complete comparisions with WIND observations. In the high resolution simulations we find:

- Ion and electron rarefaction waves (also simulated by *Farrell et al.*, [1998]).
- Two potential wells on both edges of the wake, trapping the majority of the electrons.
- Time fluctuations in the potential correlated with the release of bursts of electrons from the wake with associated E fluctuations.
- Electron two-stream instability trapping electrons in the centre of the wake.
- Dynamics of the ions are governed by electric potentials created by the electrons.
- Only the most energetic ions enter the wake, creating counter-streaming ion beams.
- Increased electron temperature in the wake.

In comparison, WIND detected: i) ion and electron rarefaction waves, ii) exponential density decreases from the wake edge to the centre, iii) counter-streaming ion beams in the wake, iv) increased electron temperature in the wake and v) electrostatic and electromagnetic waves in and near the wake.

Variations in solar wind parameters while WIND was passing through the wake highlight a limitation of these simulations. The angle between the IMF and solar wind flow varied between 5° and 60°, with the magnitude of the IMF also changing. This compares to the simulations where the angle is constrained to be 90° and magnitude constant. In order to simulate more closely the solar wind parameters during WIND's encounter with the lunar wake, and other conditions, two dimensional simulations are being undertaken.

Acknowledgments. This work was funded by PPARC and HEFCE and included usage of the GRAND and CSAR T3E facilities.

References

Bale, S. D., et al., Evidence of currents and unstable particle distributions in an extended region around the lunar plasma wake, *Geophys. Res. Lett., 24,* 1427-1430, 1997.

Bale, S. D., Shadowed particle distributions near the Moon, *J. Geophys. Res., 102,* 19,773-19,778, 1997.

Bosqued, J. M., et al., Moon-solar wind interaction: First results from the WIND/3DP experiment, *Geophys. Res. Lett., 23,* 1259-1262, 1996.

Farrell, W. M., et al., Upstream ULF waves and energetic electrons associated with the lunar wake: Detection of precursor activity, *Geophys. Res. Lett., 23,* 1271-1274, 1996.

Farrell, W. M., et al., Electrostatic instability in the central lunar wake: A process for replenishing the plasma void?, *Geophys. Res. Lett., 24,* 1135-1138, 1997.

Farrell, W. M., et al., A simple simulation of a plasma void: Applications to Wind observations of the lunar wake, *J. Geophys. Res., 103,* 23,653-23,660, 1998.

Kellogg, P. J., et al., Observations of plasma waves during a traversal of the moon's wake, *Geophys. Res. Lett., 23,* 1267-1270, 1996.

Ogilvie, K. W., et al., Observations of the lunar plasma wake from the WIND spacecraft on December 27, 1994, *Geophys. Res. Lett., 23,* 1255-1258, 1996.

Owen, C. J., et al., The lunar wake at 6.8 R_L: WIND magnetic field observations, *Geophys. Res. Lett., 23,* 1263-1266, 1996.

P. C. Birch and S. C. Chapman, Space and Astrophysics Group, Physics Dept., University of Warwick, Coventry, CV4 7AL, UK. (e-mail: birch@astro.warwick.ac.uk)

(Received June 27, 2000; revised September 6, 2000; accepted September 20, 2000.)